NATIONAL ADVISORY COMMITTEE FOR AERONAUTICS

TECHNICAL NOTE 3082

EXPERIMENTAL INVESTIGATION OF THE PURE-BENDING STRENGTH OF 75S-T6 ALUMINUM-ALLOY MULTIWEB BEAMS WITH FORMED-CHANNEL WEBS

By Richard A. Pride and Melvin S. Anderson

Langley Aeronautical Laboratory
Langley Field, Va.

Washington
March 1954

NATIONAL ADVISORY COMMITTEE FOR AERONAUTI

TECHNICAL NOTE 3082

EXPERIMENTAL INVESTIGATION OF THE PURE-BENDING STRENGTH OF 75S-T6 ALUMINUM-ALLOY MULTIWEB BEAMS WITH FORMED-CHANNEL WEBS

By Richard A. Pride and Melvin S. Anderson

SUMMARY

Experimental results are presented for the pure-bending strength of 53 multiweb beams of various proportions. The beams were fabricated from 75S-T6 aluminum-alloy sheet material and had channel-type webs which had been cold formed with bend radii of four times the web thickness. Local and wrinkling modes of buckling were observed prior to failure. All failures occurred with the formation of a trough in the compression skin extending across the web attachment flanges. The stress levels achieved at buckling and failure are discussed in terms of existing theory. Based upon the failure stresses, design charts are presented which permit rapid selection of the most efficient proportions for given values of an appropriate structural index.

INTRODUCTION

A current investigation by the Langley Structures Research Division is concerned with obtaining experimental data on the strength characteristics of thin wings with thick cover skins under various loadings. One phase of the investigation is devoted to the study of multiweb construction in which the cover skins are stabilized by equally spaced full-depth spanwise webs.

Multiweb-beam specimens representing structural sections of small absolute depth, such as are used in stabilizers and thin-wing sections, have been tested under a pure bending moment. These specimens were fabricated from 75S-T6 aluminum-alloy sheet and tested to evaluate the structural behavior and efficiency obtainable in multiweb construction using channel-type webs formed from sheet material.

This paper presents the experimental results for 53 beams of various proportions. The effects of varying the depth, spacing, and thickness of

the webs on the mode of buckling and the failing strength are described. Charts are also presented which, within the range of these tests, permit the design of the most efficient multiweb beam with formed-channel webs to meet given design requirements.

SYMBOLS

Symbols for dimensions of test specimens listed below are also shown in figure 1.

A_i average cross-sectional area per chordwise inch, consisting of area of compression skin over one cell plus one-half the area of one web, all divided by the cell width, sq in./in.

b_S web spacing, the distance from a point halfway between one rivet line and web midplane to the corresponding point halfway between next rivet line and web midplane, in.

b_W web depth measured between center lines of attachment flanges, in.

c beam width, in.

d_R rivet diameter, in.

F_1 distance from rivet line to back of web, in.

F_2 width of attachment flange, in.

h center-line depth of beam, outside depth minus thickness of one skin, in.

I moment of inertia of beam cross section, $in.^4$

L length of beam measured inside of end fixtures, in. (see fig. 2)

M_{cr} bending moment at buckling, in-kips

M_f bending moment at failure, in-kips

M_i bending moment at failure per chordwise inch of multiweb beam, in-kips/in.

p_R rivet pitch, in.

r_W radius of bend between web and attachment flange, in.

t_s skin thickness, in.

t_w web thickness, in.

σ_{cr} average stress in cover skin at buckling, $M_{cr}h/2I$, ksi

$\bar{\sigma}_f$ average stress in cover skin at failure, $M_f h/2I$, ksi

SPECIMENS

A multiweb cross section representative of 49 of the 53 tested beams is shown in figure 1. Each of these beams had a constant depth and consisted of three cells (four webs). The remaining four beams (specimens 36, 37, 38, and 39 in table I(b)) had 1, 3, 5, and 7 cells, respectively, with the flanges of all the webs turned in the same direction. All beams were fabricated from nonclad 75S-T6 aluminum-alloy sheet with compressive yield stresses varying from 69.5 ksi to 75.3 ksi with an average yield stress of 72.2 ksi. Numerous individual measurements of beam dimensions were taken on each beam before testing, and averages of these dimensions are given in table I.

Three-cell beams were assumed to give a good indication of multiweb behavior. The validity of this assumption was borne out by tests on beams with different numbers of cells, the results of which are presented in figure 3. The use of more than three cells produces insignificant changes in the buckling and failing stresses of the beams.

The length of the test section was designed to be five times either the web spacing or the web depth, whichever dimension was larger, in order to allow the free formation of a buckle pattern. At each end of the beam beyond the test section, three angle-section upright stiffeners were riveted to each web to stiffen the beam near the points of application of the bending moment. Lengths given in table I were measured between the inside edges of the end fixtures (see fig. 2).

The width of the specimen was $3b_s$ plus the additional width for two attachment flanges. Web spacing b_s was defined as the distance from a point halfway between one rivet line and web midplane to the corresponding point halfway between the next rivet line and web midplane (see fig. 1). This method of defining web spacing enables a good correlation to be made between the local buckling stress calculated by the method of reference 1 and the experimental buckling stress for those beams that developed local buckling.

Channel-type webs formed from flat sheet, which is the type used in this investigation, require a bend between the web and the attachment flanges. A preliminary check on the effect of varying the bend radius, which in turn changes the eccentricity of the rivet line, indicated significant changes in the beam failing strength (ref. 2). Changing the bend radius from $4t_W$ to $6t_W$ reduced the failing strength by 15 percent for the beams tested. Because of the appreciable detrimental effect of larger bend radii on strength and because the 75S-T6 aluminum-alloy webs could be consistently cold formed to a bend radius of $4t_W$ without cracking, the beams of this investigation were fabricated with a bend radius of $4t_W$.

Cover skins and webs were joined by strongly riveted connections through the web attachment flanges. The diameter and pitch of the A17S-T4 aluminum-alloy flat-head rivets used are given in table I and were selected on the following basis for strong riveting:

$$d_R = t_S + t_W \tag{1}$$

$$p_R = 3d_R \tag{2}$$

Equations (1) and (2) are based on past experience with stiffened panels and indicate the rivet diameter and pitch which will develop the potential strength of the structure (ref. 3). Additional tests of a few beam cross sections have indicated significant effects due to variations in the riveting. Increasing the rivet pitch produced a decrease in failing strength. Keeping a rivet pitch of 3 diameters, holding the rivet line as close to the bend radius as production would permit, and making small changes in rivet diameter produced no significant effect upon the failing strength of the beams. Rivet lines were located $1\frac{1}{2}$ rivet diameters from the edge of the web attachment flanges. Attachment-flange width was designed by the following formula:

$$F_2 = t_W + r_W + \frac{1}{32} + 2.5d_R \tag{3}$$

Use of this formula keeps the riveting as close to the plane of the webs as the corner radii permit, with a 1/32-inch tolerance for variations in fabrication.

Beams were fabricated with three nominal ratios of web thickness to skin thickness $\left(t_W/t_S = 0.27,\ 0.41,\ \text{and}\ 0.63\right)$. For each thickness ratio,

three ratios of web spacing to skin thickness (b_S/t_S = 25, 30, and 40) and five ratios of web depth to web thickness (b_W/t_W = 30, 40, 60, 80, and 120) were designed. In addition, for $t_W/t_S = 0.41$, beams of $b_S/t_S = 60$ were designed in each of the five depths.

INSTRUMENTATION AND TEST TECHNIQUES

Strains were measured at various locations on the specimens by means of Baldwin SR-4 wire resistance strain gages. Continuous records of strain against applied bending moment were obtained up to failure.

Longitudinal strains measured on the tension and compression skins indicated the overall beam response to the applied bending moment prior to buckling and were used to detect buckling on the compression skin. On most of the specimens, compression-skin gages were placed back to back in order that a strain reversal would be detected regardless of the side of the sheet on which strain reversal occurred. For the few beams where web buckling was expected prior to skin buckling, gages were mounted back to back on the webs.

Moment-strain records typical of the multiweb beams tested are reproduced in figure 4. The buckling moment was defined as the moment at which there was a vertical tangent to the moment-strain curve (marked as M_{cr} in fig. 4(a)). When a number of gages showed reversal, consideration was given to the location of the gages with respect to the buckle pattern. Only the moments indicated by those gages closest to the buckle crests (or troughs) were averaged for a determination of buckling moment. The difference in initial slope of the moment-strain curves for back-to-back gages on the compression skin (fig. 4(a)) is due to the difference in their respective distances from the neutral axis of the beam.

For a few of the beams, strain reversal was not indicated either because back-to-back gages were all located near transverse nodes of buckles, or because gages were located only on one side of the compression skin and did not show a reversal. In both of these instances (as in the right-hand curve of fig. 4(a)), buckling was defined as the point at which the strain deviated sharply from its linear relationship with moment since this point is close to the strain-reversal moment for back-to-back gages. Where no definite break in the curve occurred, buckling is given in table I by a bracketing range of stress values.

In order to measure the crushing forces present in the beam webs, strain gages were placed on the neutral axis of one exterior and one interior web of each beam and in the direction of the crushing strain.

Back-to-back gages were used so that the crushing strain could be separated from transverse bending strains (fig. 4(b)) which result from eccentrically applied crushing forces. The gages were centered on the neutral axis to minimize the components of longitudinal strain due to bending of the web in its plane.

TESTING PROCEDURE

Before testing began, the ends of the multiweb specimens were bolted to heavy end plates. This assembly was then placed in the combined load testing machine of the Langley structures research laboratory, and the end plates were bolted to the T-slotted heads of the machine (see fig. 2).

During a test, pure-bending load was applied continuously at a rate which produced an increase in compression stress in the skin of from 1 to 5 ksi per minute. All other components of load were kept at zero during a test. Failing moments were taken as the maximum moment which the specimen supported and were measured with an accuracy of ±1 percent.

RESULTS AND DISCUSSION

Buckling.- Two distinct modes of buckling occurred in the 53 multiweb beams, and the stresses associated with these modes are given in table I. In 15 of the beams, the joints between the webs and the skins behaved as unyielding supports having rotational restraint, and local buckling of the plate elements occurred with longitudinal nodes along the skin-web joints. This mode of buckling corresponds to the theory of reference 1. Five of the beams which developed local buckling had a thickness ratio of 0.63 and $b_s/t_s = 40$. The remaining 10 beams had a thickness ratio of 0.41 and $b_s/t_s = 40$ and 60.

In 38 of the 53 beams, a mode of buckling occurred in which only transverse nodes appeared on the compression skin at a spacing which varied from 0.8 to 1.2 times the web spacing. This buckling is denoted as wrinkling. The wrinkling mode has been observed previously in sandwich construction where the face plates develop short-wave-length transverse wrinkles when the stiffness of the core material in the thickness direction is low. Wrinkling in multiweb construction is similarly associated with depthwise flexibility of the supporting webs. Reference 4 brings out the importance of an effective rivet offset distance in evaluating this flexibility and presents a simple method for calculating wrinkling stresses in multiweb beams.

The correlation between calculated and experimental buckling stresses is shown in figure 5. Reasonable agreement is obtained for the beams of this test program if the effective rivet offset is taken as the distance between the web midplane and the near edge of the shanks of the rivets. The theory of reference 1 is used for those beams which buckled locally, and the theory of reference 4 is used for wrinkling. For the beams with the deepest webs $(b_W/t_W = 120)$, buckling was initiated by the webs and was adequately predicted by the theories of references 1 and 4.

Crushing effects.- Web crushing stresses measured in the multiweb beams prior to buckling were small both in absolute magnitude and in relation to their critical values. Interior webs developed about twice as much stress as exterior webs. The moment-strain record for an interior web of one of the beams developing the most crushing stress is shown in figure 4(b). The agreement shown between experimental web crushing strain and calculated strain is typical for most of the specimens.

Cross-sectional distortions.- Dial-gage measurements made on the center cross section of a typical beam as it was loaded to failure indicated the absence of any appreciable overall cross-sectional-shape change prior to buckling. Subsequent checks on other beams by visual observation with a straight edge laid across the compression skin also indicated an absence of overall shape change. A slight dishing of both tension and compression skins between webs was evident in the beams with large values of b_g/t_g, as would be expected due to the action of the crushing forces.

Failing stress.- Regardless of whether local buckling or skin wrinkling occurred, all the specimens failed with the formation of a short-wave-length trough which extended completely across the compression cover of the beam. This mode of failure was associated with a local collapse of the web in the region of the bend radius. No rivet failures occurred. Because of the localized nature of the failure, the addition of upright stiffeners to the webs of these beams would appear to have had little effect on the beam strength unless the upright spacings were very small.

The 38 beams which developed wrinkling in the skin failed at stresses less than 125 percent of the skin wrinkling stress. Thus, for multiweb beams of these proportions which develop skin wrinkling, designing on the basis of a failure load equal to 150 percent of the limit load will result in a wing structure which has buckle-free skin under all design flight conditions. The 15 beams which developed local skin buckling had larger differences between buckling and failure, with the difference depending on the buckling stress level.

Prior to buckling, beam behavior as evidenced by strain-gage readings was in good agreement with elementary beam theory. Because the wrinkling mode of buckling does not produce any appreciable redistribution of stress

at any one cross section, the failing stresses for beams which developed wrinkling were evaluated by

$$\bar{\sigma}_f = \frac{M_f h}{2I} \tag{4}$$

Beams which buckle locally, however, undergo a considerable redistribution of stress in the skin before failure, which builds up the stress in the regions of skin adjacent to the webs. Because there was one more web than there were cells, the total moment for beams which buckled locally was reduced by the amount carried by one web and beam overhang after the stress buildup, and the moment of inertia was correspondingly reduced. The moment carried by one web was computed from strains measured by long strain gages (Baldwin SR-4 type A-9) placed on the skin over the webs.

The average stress in the skin at failure for 75S-T6 aluminum-alloy multiweb beams with formed-channel webs with a bend radius of $4t_w$ is shown in figures 6 to 8 and is listed in table I for the specimens tested. The symbols are experimental values, adjusted for the beams that developed local buckling, and the curves (based on several types of cross plots) are faired to give the best fit to the experimental data.

Failing stress $\bar{\sigma}_f$ is plotted against the ratio of beam thickness to skin thickness h/t_s, since these dimensions are usually fixed by initial design considerations. Results for ratios of web thickness to skin thickness t_w/t_s of 0.27, 0.41, and 0.63 are shown in figures 6, 7, and 8, respectively. The curves indicate that, for any given web spacing b_s, the failing stress is reduced slightly as the beam depth increases. This stress decrease results from a deflectional-stiffness decrease in the formed-channel webs as the depth increases. Higher failing stresses result from closer web spacing and increased web thickness. With respect to the general stress level achieved at failure, it was noted that, for many of the beams which developed skin wrinkling, the failing stresses were less than the buckling stresses predicted by references 1 and 5 for integral structures of the same dimensions.

Design charts.- From aerodynamic considerations, a general airfoil shape is usually specified so that the structural design has given values of applied bending moment per chordwise inch M_1 and beam depth h, where h is the distance between center lines of the tension and compression skins. In addition, a minimum skin thickness t_s may be specified for torsional stiffness. Design charts incorporating these quantities are presented in figures 9 to 11 for 75S-T6 aluminum-alloy multiweb beams with channel-type webs formed with a bend radius of $4t_w$. Figures 9, 10,

and 11 are for ratios of web thickness to skin thickness t_W/t_S of 0.27, 0.41, and 0.63, respectively, and present M_i/h^2 as a function of h/t_S for values of b_S/t_S of 25, 30, and 40. The design curves shown were calculated from the experimental curves of average skin stress at failure (figs. 6 to 8).

When figures 9, 10, and 11 are entered with a fixed value of M_i/h^2, various combinations of b_S/t_S, t_W/t_S, and h/t_S can be obtained for a variety of cell proportions, any of which will carry the design load at the design depth. The most efficient of these combinations will be the one with the smallest cross-sectional area. The cross-sectional area of the beams in this investigation is expressed as a nondimensional ratio A_i/t_S where

$$\frac{A_i}{t_S} = 1 + \frac{0.5t_W/t_S}{b_S/t_S}\left(\frac{h}{t_S} + 9.14\,\frac{t_W}{t_S} + 4\right) \tag{5}$$

For $t_W/t_S = 0.27$,

$$\frac{A_i}{t_S} = 1 + \frac{0.135}{b_S/t_S}\left(\frac{h}{t_S} + 6.47\right) \tag{6}$$

for $t_W/t_S = 0.41$,

$$\frac{A_i}{t_S} = 1 + \frac{0.205}{b_S/t_S}\left(\frac{h}{t_S} + 7.75\right) \tag{7}$$

and for $t_W/t_S = 0.63$,

$$\frac{A_i}{t_S} = 1 + \frac{0.315}{b_S/t_S}\left(\frac{h}{t_S} + 9.76\right) \tag{8}$$

The use of the design charts and equations (5) to (8) is shown in the illustrative examples.

Efficiency chart.- When a particular structural configuration is proposed to satisfy aerodynamic, structural, and production requirements, it frequently is useful to know how the compromise design compares with

the most efficient design that would be obtainable without satisfying all the requirements. One type of beam efficiency chart is shown in figures 12 and 13. The average stress level in the compression half of a beam M_1/A_1h is given in terms of a structural loading index M_1/h^2. The most efficient beam for a given depth and moment will be the one developing the highest average stress.

For each value of t_W/t_S, the most efficient test specimens were those having a value of $b_S/t_S = 25$. Figure 12 shows the effect on the efficiency of a variation in the ratio b_S/t_S for $t_W/t_S = 0.63$ and is typical of the other thickness ratios. Figure 13 presents the efficiency curves for each of the thickness ratios at a value of $b_S/t_S = 25$, and, as can be seen, the thickness ratio $t_W/t_S = 0.63$ is the most efficient over the range of the experimental program. Since values of $b_S/t_S = 25$ and $t_W/t_S = 0.63$ also correspond to limiting values of these parameters in the experimental program, it is not obvious that they are the most efficient that could be obtained with the formed-channel type of construction. However, extrapolation of the failing stresses as functions of the ratios t_W/t_S and b_S/t_S as well as a study of predictions based on the theory of reference 4 indicates that close to peak efficiency is obtained at values of $t_W/t_S = 0.63$ and $b_S/t_S = 25$.

These efficiency curves show that, for multiweb beams with formed-channel webs, the most efficient proportions do not correspond to those found in references 1 and 5. In references 1 and 5, local buckling and a mode of failure associated with local buckling were assumed to occur, whereas the beams of the present investigation failed in a mode associated with wrinkling.

Efficiency charts such as figures 12 and 13 are useful not only for comparing various multiweb designs but also for comparing other types of skin stabilization such as stiffened-panel or multipost stiffened construction. Such comparisons should serve as a guide in determining the limits of efficient wing construction for each type of internal structure. Design of multiweb beams on an efficiency basis is illustrated in the following section.

ILLUSTRATIVE EXAMPLES

By use of the design charts (figs. 9 to 11) two examples are worked; each gives the most efficient design for the stipulated conditions of the problem.

Example 1.- From aerodynamic considerations, M_i is required to be at least 37.5 in-kips/in., and an average beam depth over the structural portion is 5 inches. In addition, a minimum skin thickness $t_s = 0.188$ inch is required to provide torsional stiffness. Thus $M_i/h^2 = 1.50$ ksi, $h/t_s = 26.6$, and b_s and t_w can be varied to give the most efficient structure.

Entering the design charts (figs. 9 to 11) with these values and using equations (6) to (8) yields the following values:

t_w/t_s	b_s/t_s	A_i/t_s	A_i
0.27	25	1.179	0.222
.41	31	1.227	.231
.63	40	1.286	.242

The structure having the smallest value of A_i will be the lightest and, therefore, the most efficient. Thus, for the stipulated conditions $M_i/h^2 = 1.50$, $h = 5$ inches, and $t_s \geq 0.188$ inch, the most efficient structure is

$$A_i = 0.222 \text{ inch}$$

$$b_s = 4.70 \text{ inches}$$

$$t_s = 0.188 \text{ inch}$$

$$t_w = 0.051 \text{ inch}$$

If the skin thickness is not restricted, a more efficient design than the one above could be obtained. As shown in figure 13, the most efficient design at $M_i/h^2 = 1.50$ is $t_w/t_s = 0.63$ and $b_s/t_s = 25$, for which $t_s = 0.121$ inch and $A_i = 0.198$ inch.

Example 2.- Redesign the beam in example 1 with the further requirement that the web spacings must be at least 6.5 inches.

Having a minumum web spacing specified as well as a minimum skin thickness leads to an initial requirement of $b_s/t_s \geq 34.6$. Since only one of the three designs in the first example satisfies this requirement

$(t_W/t_S = 0.63, \quad b_S/t_S = 40)$, a heavier skin will be required for trial designs having values of $t_W/t_S = 0.27$ and 0.41. Using the next heavier standard gage $t_S = 0.250$ inch requires values of $h/t_S = 20.0$ and $b_S/t_S \geq 26.0$.

In a manner similar to that in the first example, the following values are obtained for $t_S = 0.250$ inch:

t_W/t_S	b_S/t_S	A_i/t_S	A_i
0.27	35	1.102	0.276
.41	40	1.142	.286

It can be seen that the use of heavier skin reduces the efficiency in this example. In the first example, as thickness ratio was decreased, efficiency increased. A plot of values of b_S/t_S against t_W/t_S shows that t_W/t_S may be as low as 0.50 when $b_S/t_S = 34.6$. Using a standard sheet gage of $t_W = 0.102$ inch gives values of $t_W/t_S = 0.54$ and $b_S/t_S = 36.0$. From equation (5), A_i can be computed to be 0.238 inch. Thus, the most efficient structure for $M_i/h^2 = 1.50$ ksi, $h = 5.0$ inch, $t_S \geq 0.188$ inch, and $b_S \geq 6.5$ inch is

$$A_i = 0.238 \text{ inch}$$
$$b_S = 6.76 \text{ inches}$$
$$t_S = 0.188 \text{ inch}$$
$$t_W = 0.102 \text{ inch}$$

which is a heavier structure than that in example 1 because of the added restriction on web spacing.

SUMMARY OF RESULTS

Experimental results have been presented for the pure-bending strength of 75S-T6 aluminum-alloy multiweb beams fabricated with channel-type webs formed with a bend radius of four times the web thickness. The following observations were made of the tests:

1. Local buckling of the plate elements and wrinkling of the entire compression skin were the two modes of buckling that occurred, and the agreement with buckling theory was satisfactory.

2. All beams failed with the formation of a trough in the compression skin across the web attachment flanges. For the type of failure experienced, no gain in strength would be expected by the addition of upright stiffeners to the webs unless the upright spacings were very small.

3. Due to the adequacy of the strongly riveted connections, no rivet failures were experienced. Increasing rivet pitch produced decreasing failing strength, but small changes in rivet diameter produced no significant change in beam failing strength.

4. Three-cell beams gave a good indication of multiweb behavior. The use of more than three cells produced insignificant changes in the buckling and failing stresses of the beams.

5. Measured crushing forces in the webs prior to buckling were in good agreement with theory and always were small.

6. The average skin stress at failure can generally be increased by any of the following: decreasing web depth, decreasing web spacing, and increasing web thickness.

Design charts presented make possible rapid selection of efficient designs. An efficiency study indicated that, for the type of beam tested, close to peak efficiency was obtained with values of the ratios of web thickness to skin thickness $t_W/t_S = 0.63$ and web spacing to skin thickness $b_S/t_S = 25$.

Langley Aeronautical Laboratory,
National Advisory Committee for Aeronautics,
Langley Field, Va., January 20, 1954.

REFERENCES

1. Schuette, Evan H., and McCulloch, James C.: Charts for the Minimum-Weight Design of Multiweb Wings in Bending. NACA TN 1323, 1947.

2. Anderson, Roger A., Pride, Richard A., and Johnson, Aldie E., Jr.: Some Information on the Strength of Thick-Skin Wings With Multiweb and Multipost Stabilization. NACA RM L53F16, 1953.

3. Dow, Norris F., Hickman, William A., and Rosen, B. Walter: Effect of Variation in Rivet Strength on the Average Stress at Maximum Load for Aluminum-Alloy, Flat, Z-Stiffened Compression Panels That Fail by Local Buckling. NACA TN 2963, 1953.

4. Anderson, Roger A., and Semonian, Joseph W.: Charts Relating the Compressive Buckling Stress of Longitudinally Supported Plates to the Effective Deflectional and Rotational Stiffness of the Supports. NACA TN 2987, 1953.

5. Gerard, George: Efficient Applications of Stringer Panel and Multicell Wing Construction. Jour. Aero. Sci., vol. 16, no. 1, Jan. 1949, pp. 35-40.

TABLE I.- DIMENSIONS OF MULTIWEB BEAMS AND TEST RESULTS

(a) $t_W/t_S = 0.27$

$\left[F_2 = 0.91 \text{ inch};\quad r_W/t_W = 4;\quad d_R = 1/4 \text{ inch};\quad p_R = 3/4 \text{ inch}\right]$

Specimen	t_W, in.	t_S, in.	b_W, in.	b_S, in.	F_1, in.	c, in.	h, in.	L, in.	I, $in.^4$	t_W/t_S	b_S/t_S	h/t_S	M_f, in-kips	σ_{cr}, ksi	$\bar{\sigma}_f$, ksi
1	0.0512	0.190	1.52	4.68	----	15.35	1.76	28.6	4.75	0.270	24.6	9.3	215	38.3	39.8
2	.0513	.184	2.04	4.68	0.56	15.40	2.28	28.6	7.80	.279	25.4	12.4	266	37.2	38.9
3	.0512	.182	3.06	4.69	.50	15.40	3.30	28.5	16.21	.281	25.8	18.1	420	42.8	42.8
4	.0515	.186	4.11	4.71	.54	15.40	4.35	28.5	30.16	.277	25.3	23.4	519	37.0	37.4
5	.0514	.186	6.14	4.69	.57	15.40	6.37	35.3	65.81	.276	25.2	34.2	650	27.5 [a]21.1	31.5
6	.0521	.190	1.54	5.65	.54	18.20	1.78	33.1	5.75	.274	29.7	9.4	217	32.2	33.6
7	.0518	.185	2.08	5.65	----	18.22	2.31	33.1	9.62	.280	30.5	12.5	276	30.4	33.1
8	.0517	.184	3.07	5.64	.54	18.20	3.30	33.0	19.55	.281	30.7	17.9	388	31.4	32.7
9	.0508	.192	6.14	5.65	.54	18.21	6.38	35.3	77.77	.265	29.4	33.2	715	25.9 [a]24.8	29.3
10	.0506	.192	1.56	7.50	.52	23.83	1.80	42.8	7.65	.264	39.1	9.4	210	23.3	24.7
11	.0508	.189	2.08	7.50	.54	23.81	2.32	42.8	12.60	.269	39.7	12.3	278	22.3	25.6
12	.0508	.189	3.09	7.48	.54	23.84	3.33	42.8	26.35	.269	39.6	17.6	388	21.5	24.5
13	.0507	.189	4.10	7.53	----	23.82	4.34	42.8	44.87	.268	39.8	23.0	498	21.8	24.1
14	.0512	.189	6.15	7.50	----	23.80	6.39	42.8	98.86	.271	39.7	33.8	745	21.8 [a]21.5	24.1

[a]Average stress in cover skin when webs buckled.

TABLE I.- DIMENSIONS OF MULTIWEB BEAMS AND TEST RESULTS - Continued

(b) $t_W/t_S = 0.41$

$\left[F_2 = 0.76 \text{ inch};\ r_W/t_W = 4;\ d_R = 3/16 \text{ inch};\ p_R = 9/16 \text{ inch}\right]$

Specimen	t_W, in.	t_S, in.	b_W, in.	b_S, in.	F_1, in.	c, in.	h, in.	L, in.	I, $in.^4$	t_W/t_S	b_S/t_S	h/t_S	M_f, in-kips	σ_{cr}, ksi	$\bar{\sigma}_f$, ksi
15	0.0504	0.125	1.55	3.12	0.49	10.42	1.73	20.6	2.14	0.403	25.0	13.8	104	36.4	42.0
16	.0505	.126	2.05	3.12	.50	10.42	2.22	20.7	3.64	.401	24.8	17.6	146	38.4	44.7
17	.0511	.125	3.08	3.12	.48	10.42	3.26	20.7	7.98	.409	25.0	26.1	212	38.8	43.3
18	.0503	.125	4.08	3.12	.44	10.41	4.26	25.2	13.91	.402	25.0	34.1	268	32.0 to 39.7	41.0
19	.0510	.126	6.15	3.14	.50	10.38	6.32	35.3	32.38	.405	24.9	50.2	394	{35.7 [a]22.8	38.5
20	.0500	.125	1.56	3.74	.48	12.27	1.74	23.5	2.50	.400	29.9	13.9	119	37.7	41.4
21	.0500	.125	2.08	3.75	.48	12.27	2.26	23.5	4.30	.400	30.0	18.1	139	33.4	36.5
22	.0502	.125	3.10	3.75	.48	12.27	3.28	23.5	9.31	.402	30.0	26.2	204	31.5	35.9
23	.0502	.126	4.08	3.75	.47	12.27	4.25	25.2	16.11	.398	29.8	33.7	265	31.7	35.0
24	.0513	.128	4.14	3.80	----	12.25	4.32	25.2	16.86	.401	29.7	33.8	292	37.0	37.5
25	.0506	.125	6.17	3.75	.48	12.27	6.35	35.3	37.15	.405	30.0	50.8	388	{28.4 [a]22.2	33.2
26	.0499	.125	1.56	4.99	----	16.06	1.74	29.7	3.22	.399	39.9	13.9	111	25.8	30.0
27	.0507	.125	2.08	5.00	----	16.06	2.26	29.7	5.52	.406	40.0	18.1	148	25.8	30.3
28	.0501	.124	3.12	5.00	.46	16.07	3.30	29.7	11.94	.404	40.3	26.6	196	22.2	27.1
29	.0506	.125	4.10	5.00	.46	16.05	4.28	29.6	20.56	.405	40.0	34.2	265	24.2	27.6
30	.0509	.125	6.17	5.00	.48	16.05	6.35	35.3	46.73	.407	40.0	50.8	385	{23.8 [a]21.2	26.2
31	.0505	.126	1.57	7.46	----	23.54	1.74	42.0	4.71	.401	59.2	13.8	124	12.0	22.4
32	.0511	.125	2.12	7.49	----	23.52	2.30	42.0	8.18	.409	59.9	18.4	156	11.3	21.4
33	.0501	.125	3.12	7.51	.48	23.52	3.30	42.0	17.06	.401	60.1	26.4	234	11.0	21.9
34	.0508	.125	4.12	7.50	.44	23.52	4.30	42.0	29.34	.406	60.0	34.4	307	11.5	21.5
35	.0499	.125	6.17	7.50	.48	23.52	6.35	42.0	65.46	.399	60.0	50.8	430	11.7	19.5
[b]36	.0509	.125	3.60	3.75	.48	4.51	3.78	23.5	4.82	.407	30.0	30.2	95	30.6	37.2
[b]37	.0519	.125	3.58	3.76	.47	12.02	3.76	23.5	12.24	.415	30.1	30.1	252	37.1	38.6
[b]38	.0507	.126	3.58	3.74	.48	19.50	3.76	23.5	19.73	.403	29.7	29.8	398	37.5	37.9
[b]39	.0514	.125	3.58	3.75	.47	27.04	3.76	23.5	27.03	.411	30.0	30.1	559	37.9	38.9

[a]Average stress in cover skin when webs buckled.

[b]Specimens 36, 37, 38, and 39 have 1, 3, 5, and 7 cells, respectively.

TABLE I.- DIMENSIONS OF MULTIWEB BEAMS AND TEST RESULTS - Concluded

(c) $t_W/t_S = 0.63$

[$F_2 = 0.60$ inch; $r_W/t_W = 4$; $d_R = 1/8$ inch; $P_R = 3/8$ inch]

Specimen	t_W, in.	t_S, in.	b_W, in.	b_S, in.	F_1, in.	c, in.	h, in.	L, in.	I, $in.^4$	t_W/t_S	b_S/t_S	h/t_S	M_f, in-kips	σ_{cr}, ksi	$\bar{\sigma}_f$, ksi
40	0.0520	0.0825	1.55	1.99	0.41	6.84	1.68	14.7	0.97	0.630	24.1	20.4	59.0	46.3	51.1
41	.0505	.0823	2.07	2.02	.40	6.84	2.20	15.1	1.70	.614	24.5	26.7	77.9	49.6	50.4
42	.0503	.0836	3.08	2.07	.42	6.85	3.22	19.9	3.95	.601	24.7	38.5	121.0	48.6	49.3
43	.0514	.0835	4.11	2.04	.41	6.84	4.25	25.2	7.14	.615	24.5	50.9	161.0	46.4	47.9
44	.0512	.0828	6.13	2.02	.40	6.80	6.26	35.3	16.72	.619	24.4	75.7	228.5	38.9 [a]24.1	42.8
45	.0519	.0830	1.55	2.41	.42	8.06	1.69	16.9	1.13	.624	29.0	20.4	61.2	39.8	45.8
46	.0499	.0828	2.07	2.44	.40	8.06	2.20	16.9	1.92	.602	29.5	26.6	76.2	33.5	43.7
47	.0507	.0839	3.08	2.49	.44	8.07	3.22	19.8	4.59	.605	29.7	38.4	116.3	39.2	40.8
48	.0512	.0825	6.16	2.45	.43	8.07	6.29	35.3	18.93	.621	29.7	76.2	211.0	30.4 [a]19.9	35.1
49	.0513	.0834	1.55	3.24	.40	10.50	1.68	21.1	1.40	.615	38.9	20.2	59.0	27.2	35.4
50	.0504	.0838	2.06	3.25	.40	10.50	2.19	21.1	2.44	.601	38.8	26.2	81.6	29.8	36.6
51	.0503	.0824	3.06	3.21	.40	10.50	3.19	21.0	5.35	.611	39.0	38.8	113.5	27.1	33.8
52	.0518	.0832	4.08	3.24	.40	10.50	4.22	25.2	9.78	.622	39.0	50.7	152.0	25.4	32.8
53	.0513	.0814	6.17	3.26	.42	10.50	6.30	35.3	22.76	.630	40.1	77.5	215.0	22.0 [a]18.3	29.8

[a]Average stress in cover skin when webs buckled.

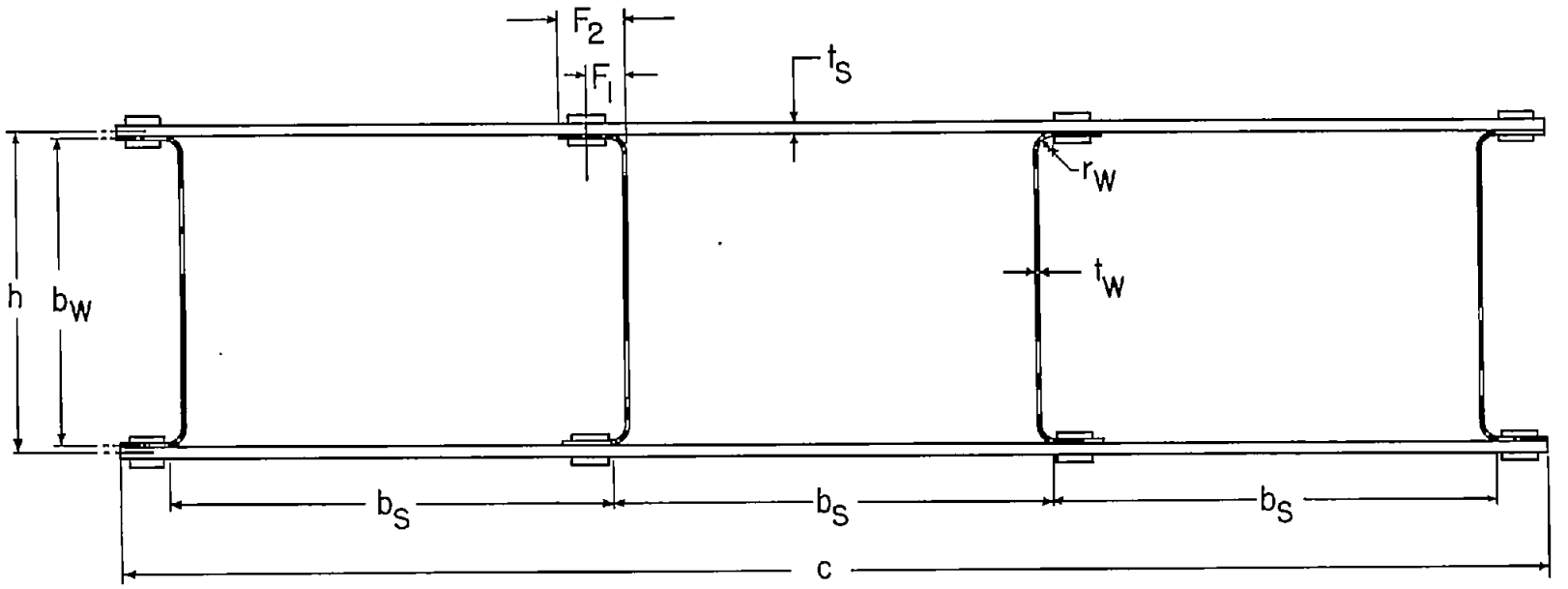

Figure 1.- Multiweb-beam cross section.

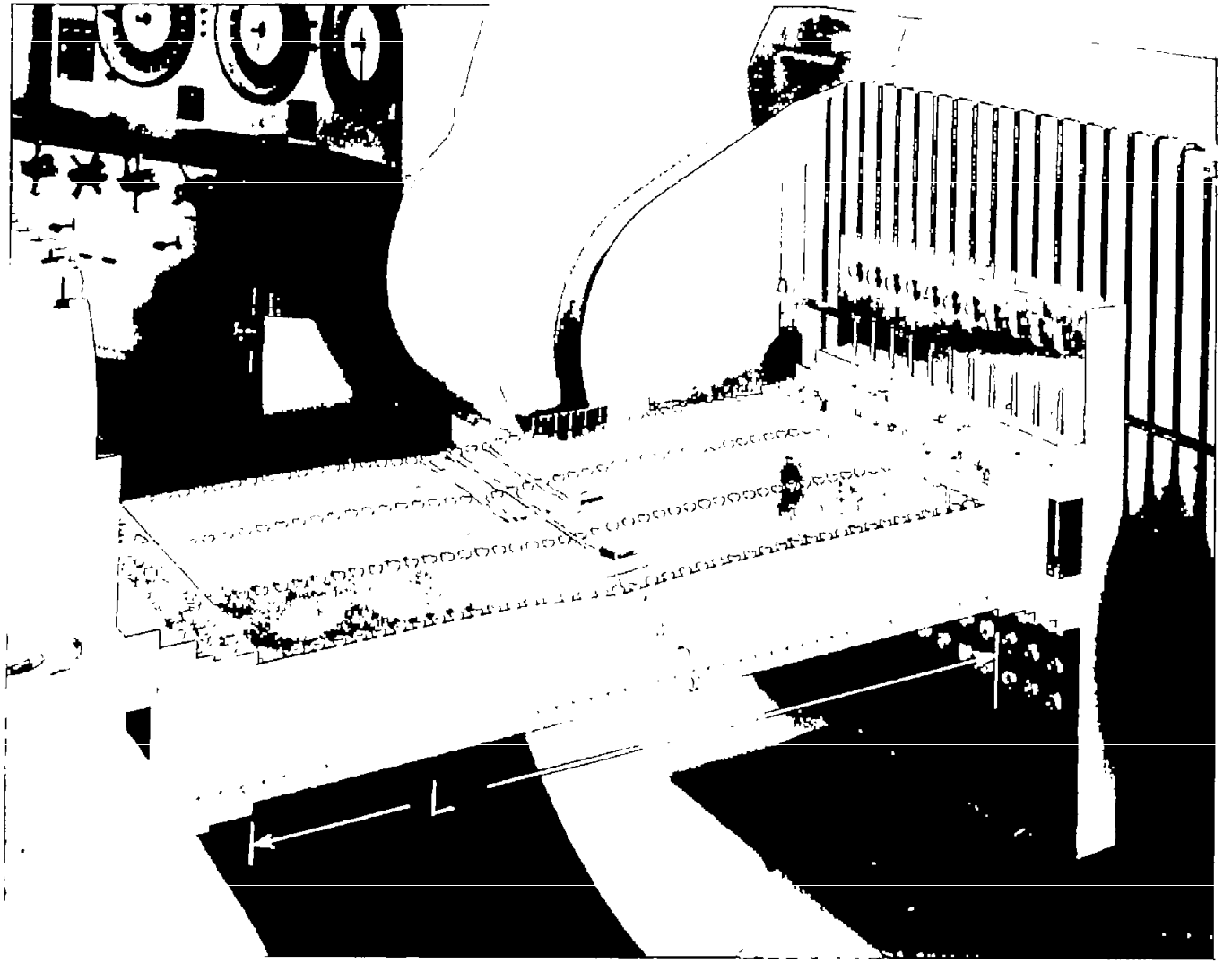

L-80428.1

Figure 2.- Multiweb beam after pure-bending failure mounted in combined load testing machine.

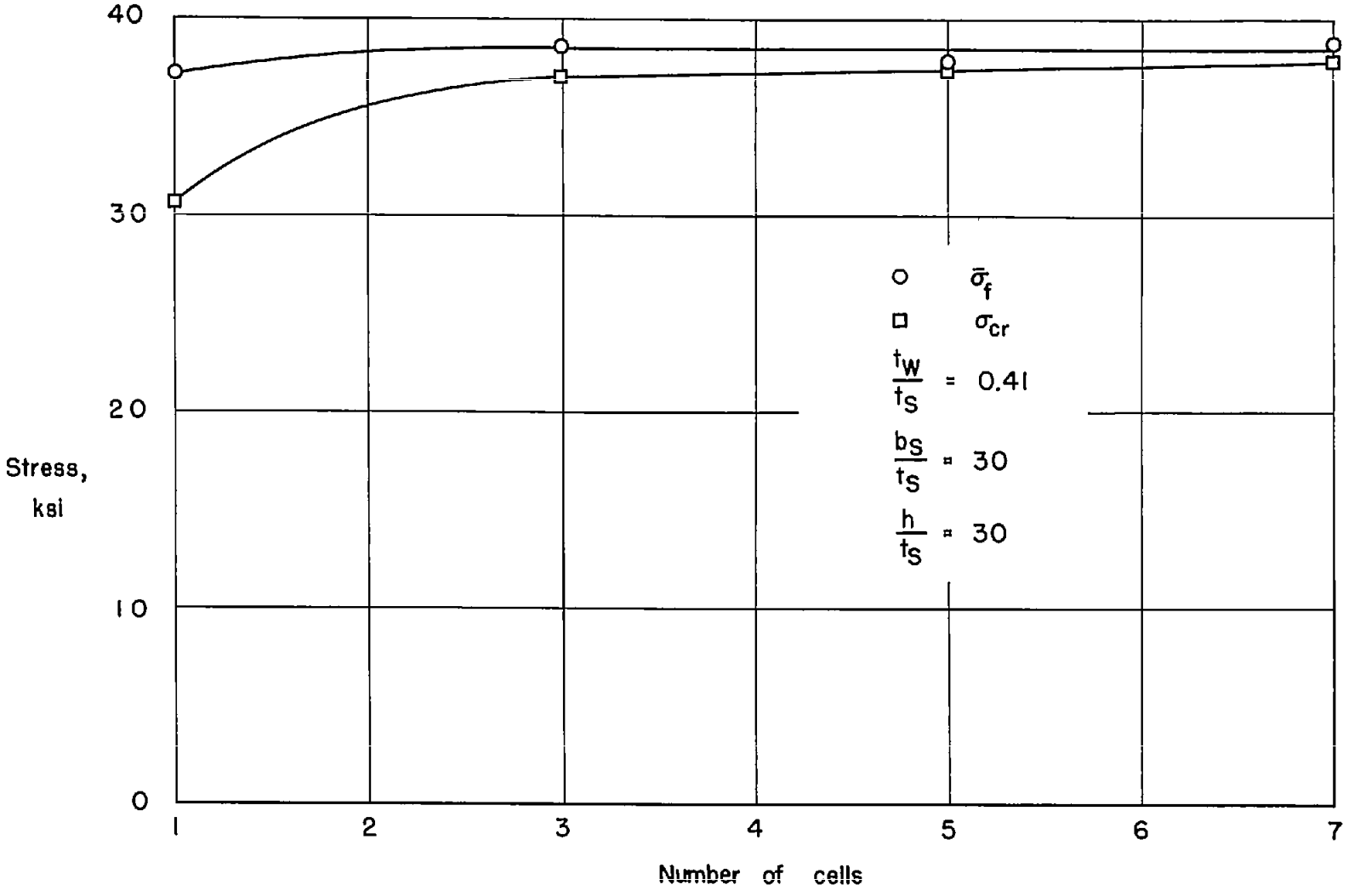

Figure 3.—Effect of variation in the number of cells on the strength of multiweb beams loaded in pure bending.

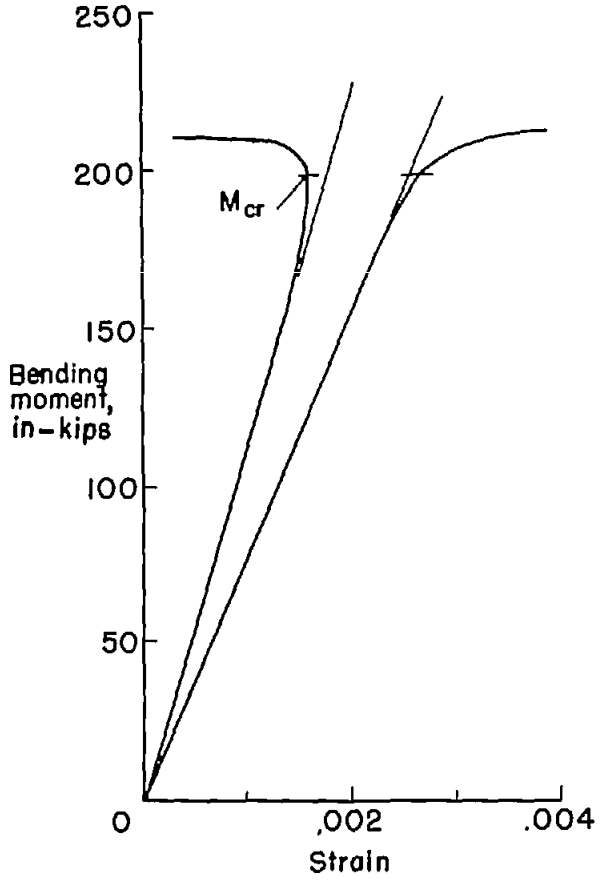

(a) Axial strain in compression cover, two gages back to back.

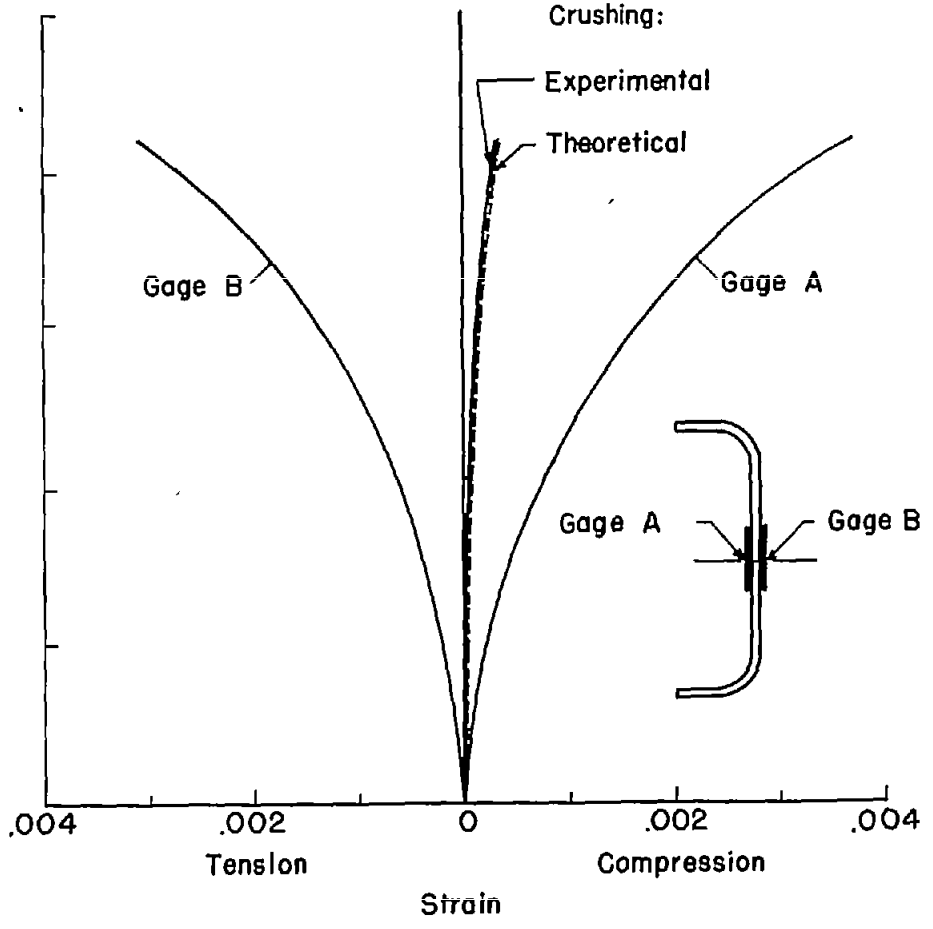

(b) Transverse strain in an interior web.

Figure 4.- Measured moment-strain relationships which are typical of multiweb beams.

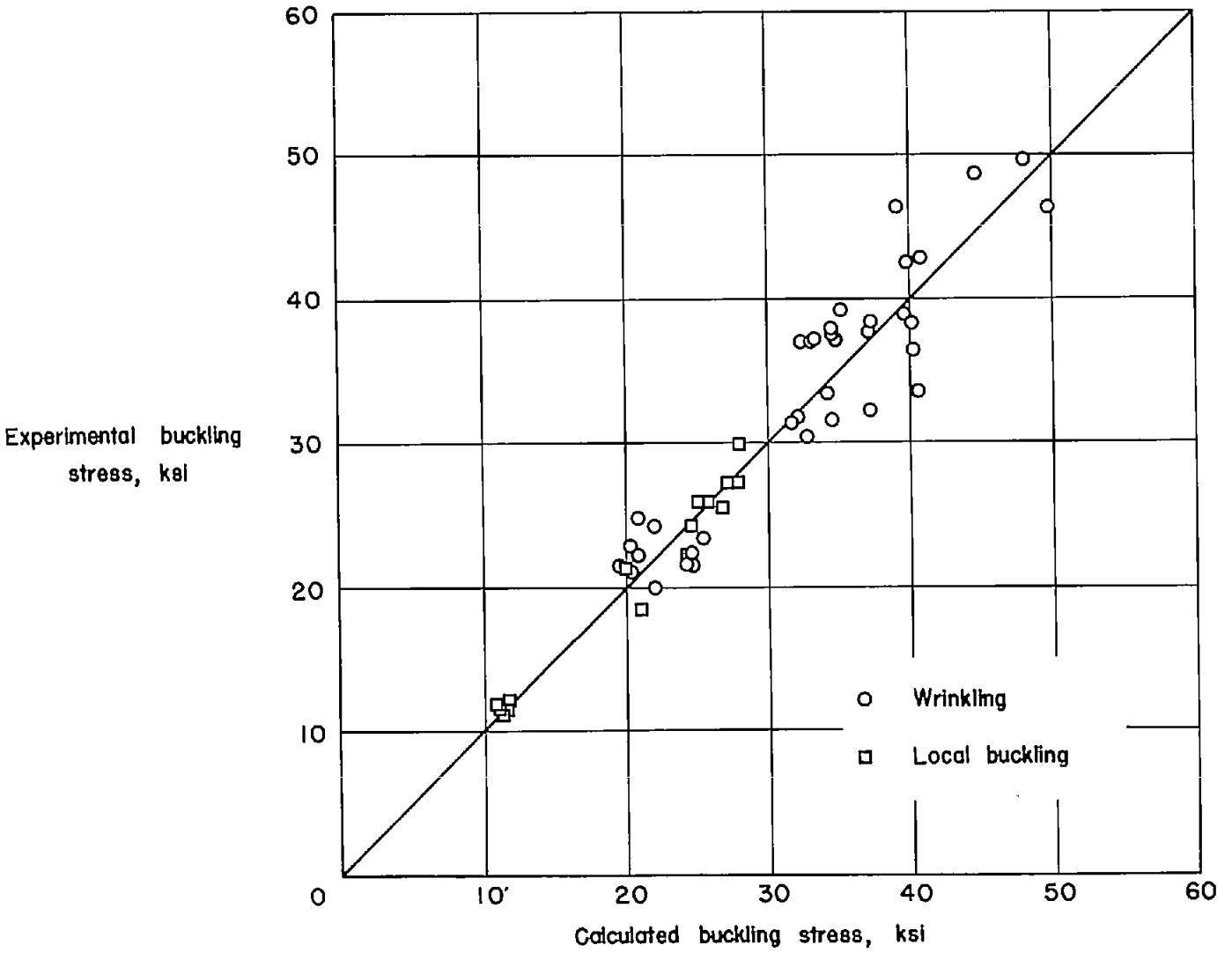

Figure 5. — Comparison of theoretical and experimental buckling stress.

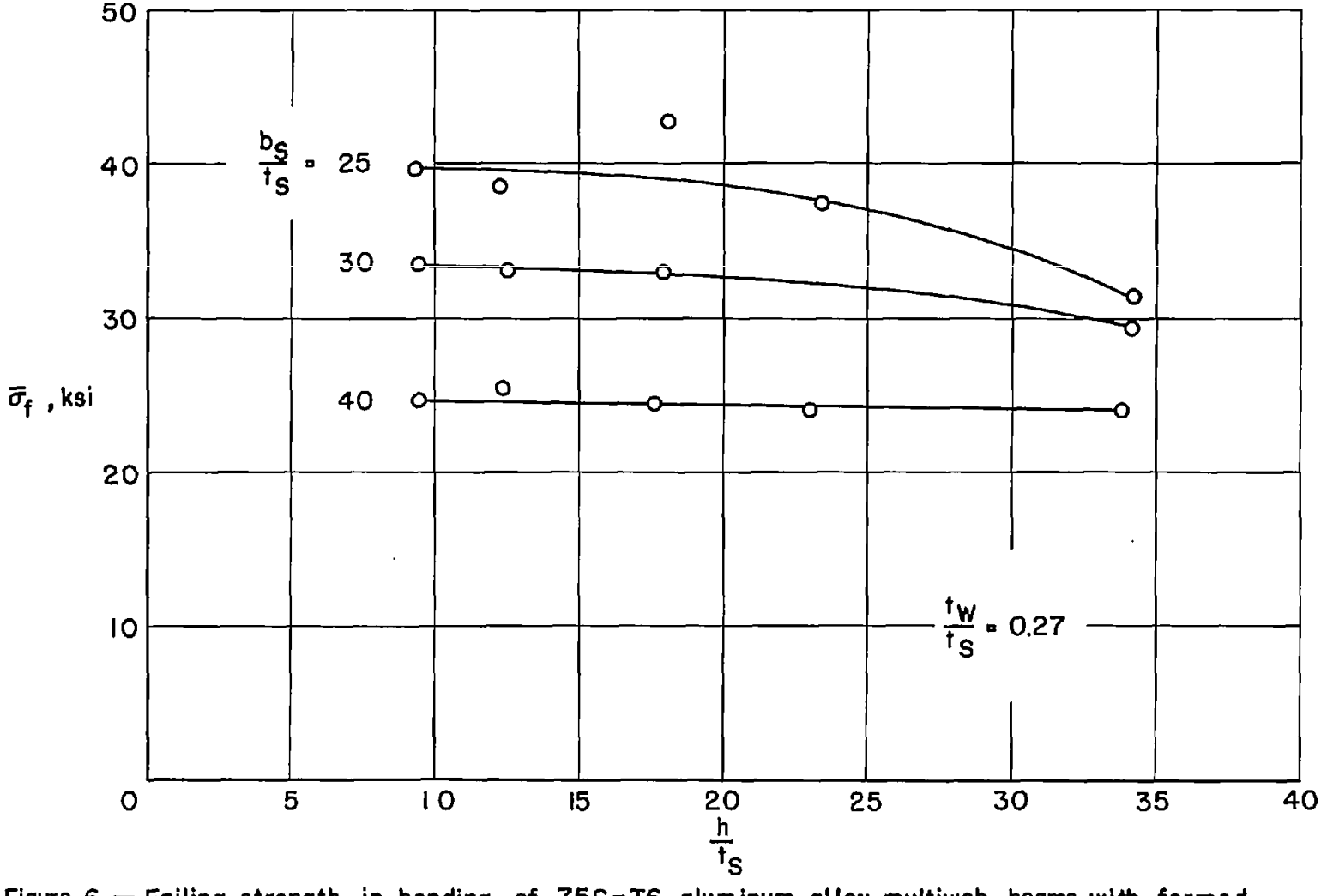

Figure 6.— Failing strength in bending of 75S-T6 aluminum-alloy multiweb beams with formed-channel webs, $\frac{t_w}{t_s}$ = 0.27.

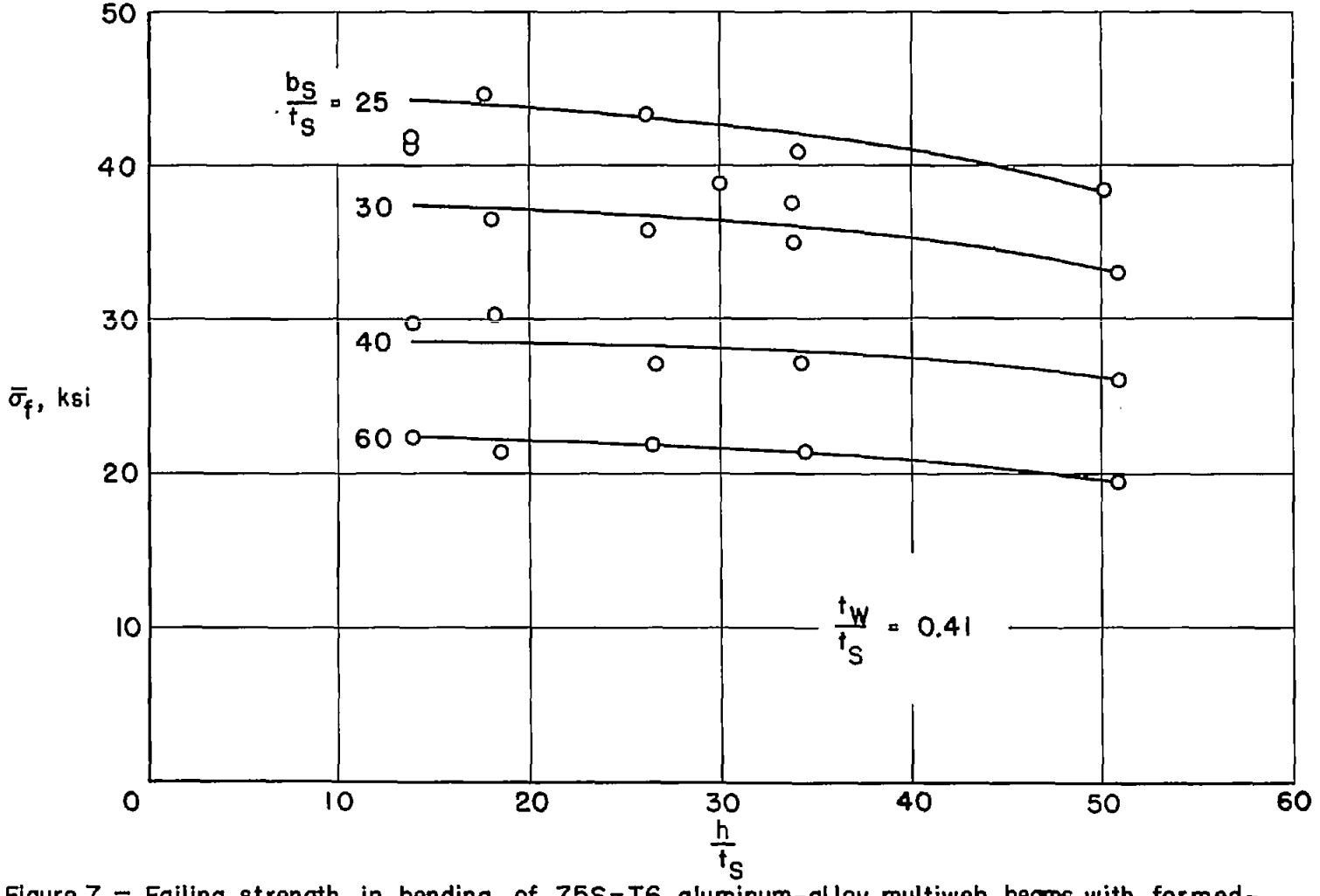

Figure 7.– Failing strength in bending of 75S-T6 aluminum-alloy multiweb beams with formed-channel webs. $\frac{t_w}{t_s} = 0.41$.

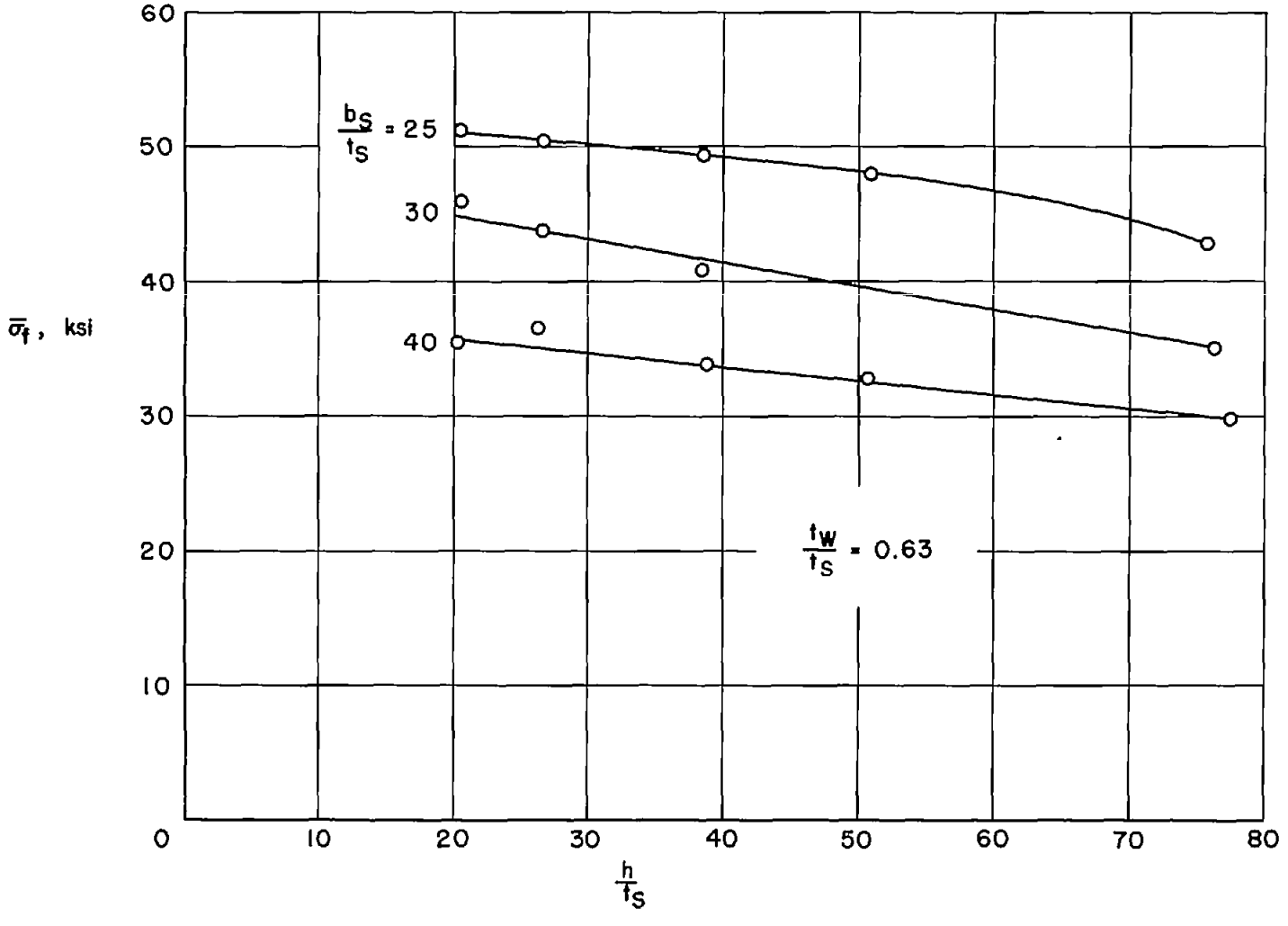

Figure 8.— Failing strength in bending of 75S-T6 aluminum-alloy multiweb beams with formed-channel webs. $\frac{t_w}{t_s} = 0.63$.

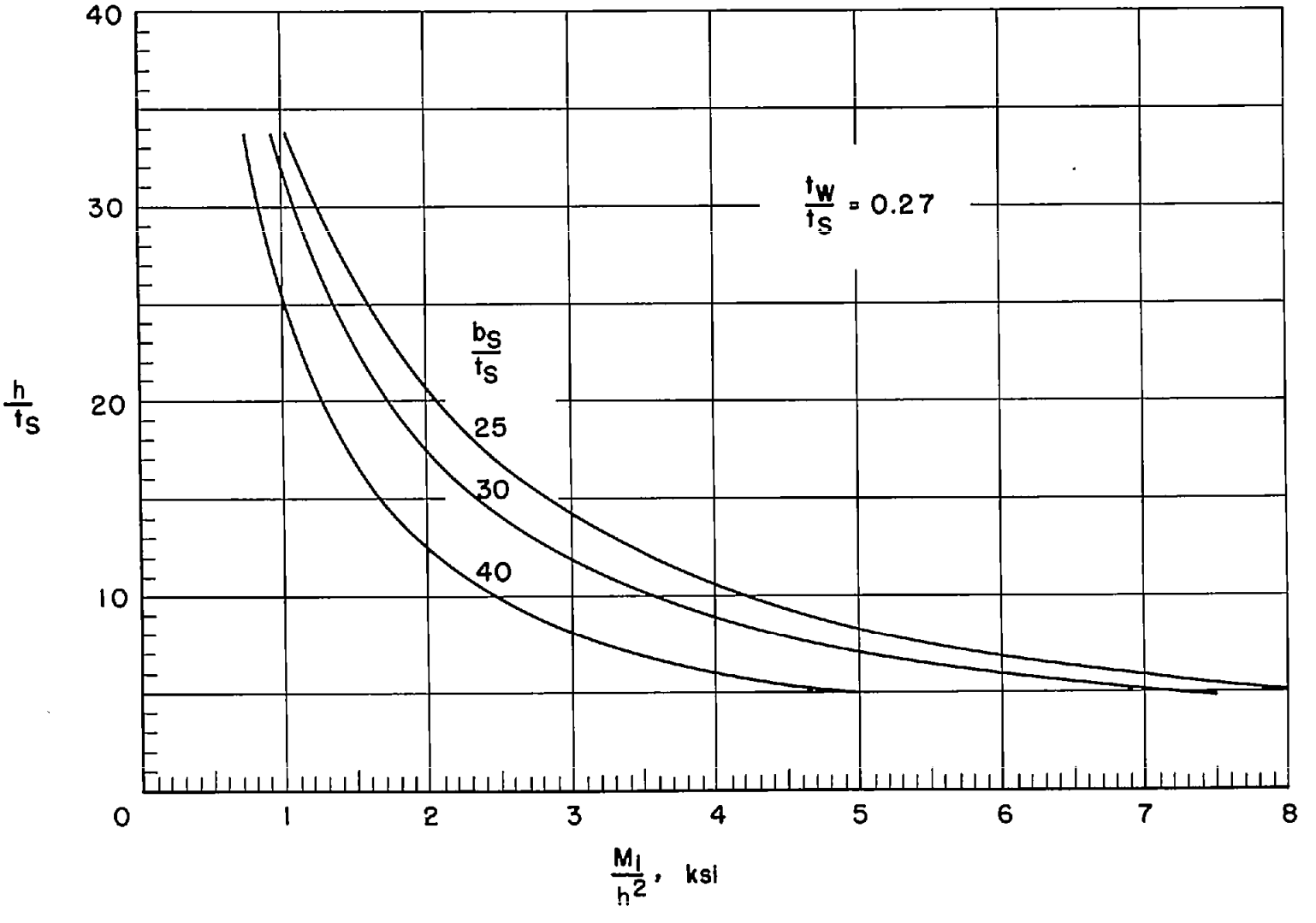

Figure 9. — Design chart for 75S-T6 aluminum-alloy multiweb beams with formed-channel webs. $\frac{t_w}{t_s} = 0.27$.

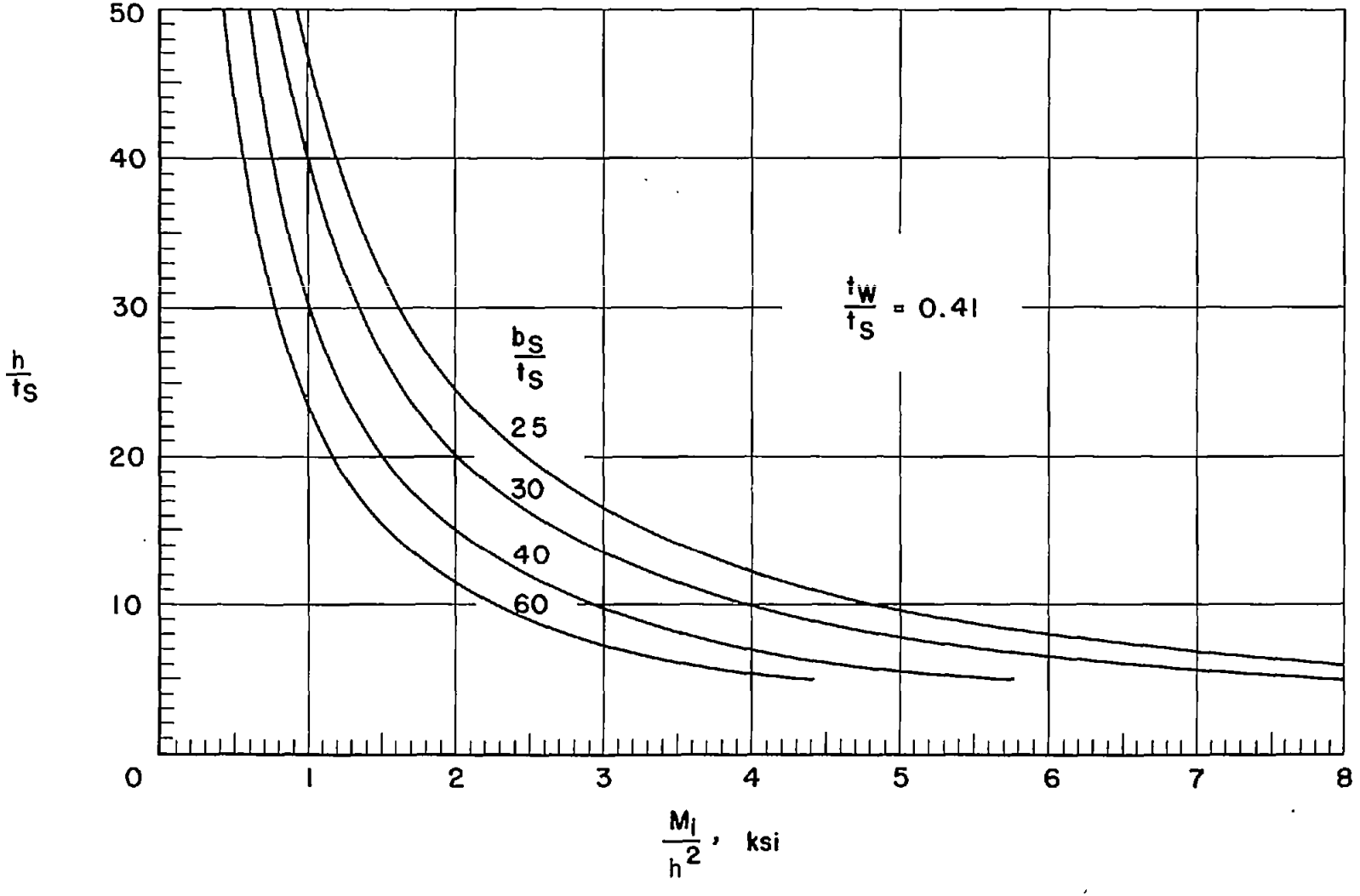

Figure 10.— Design chart for 75S-T6 aluminum-alloy multiweb beams with formed-channel webs. $\frac{t_W}{t_S}$ = 0.41.

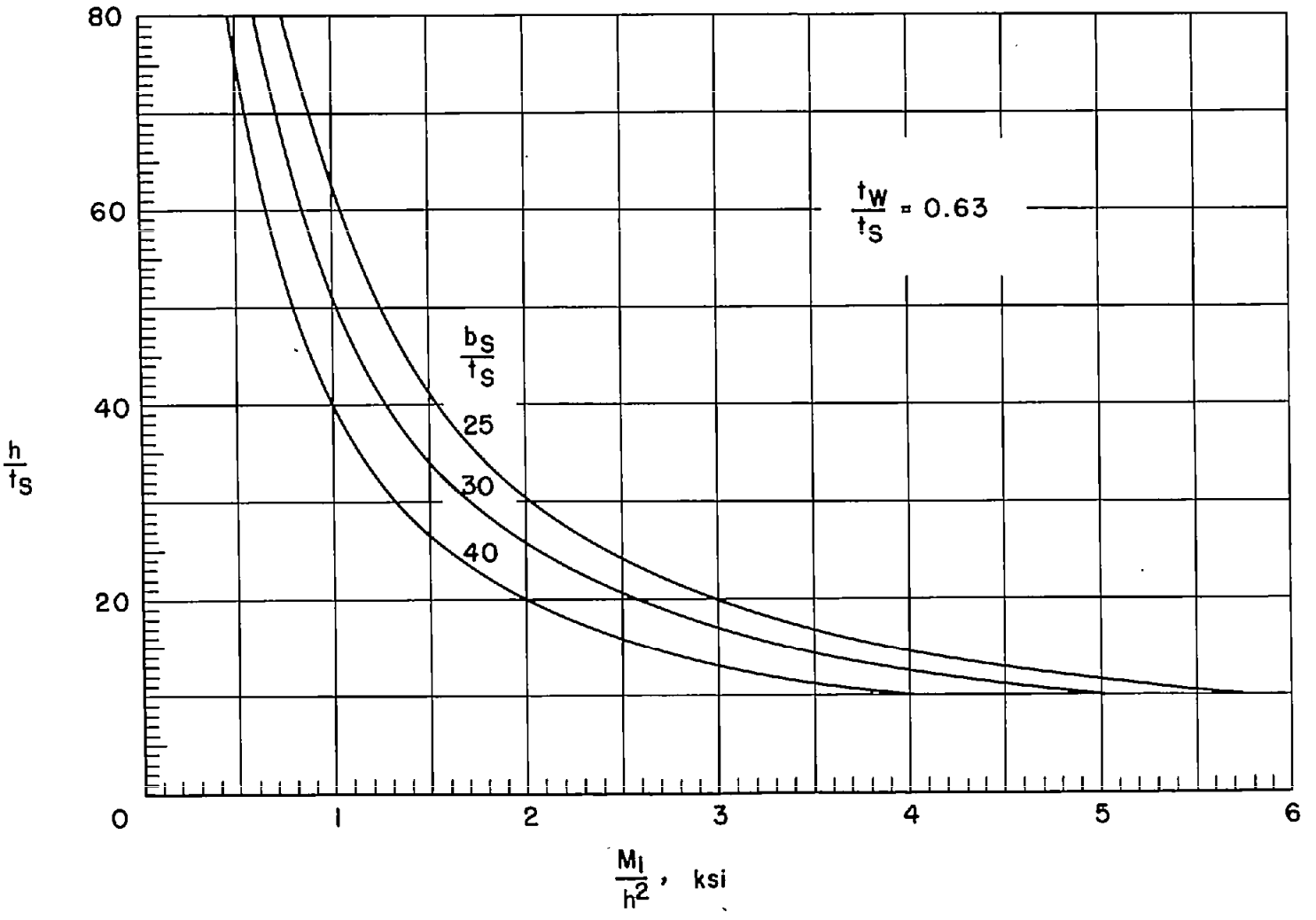

Figure 11.— Design chart for 75S-T6 aluminum-alloy multiweb beams with formed-channel webs $\frac{t_w}{t_s} = 0.63$.

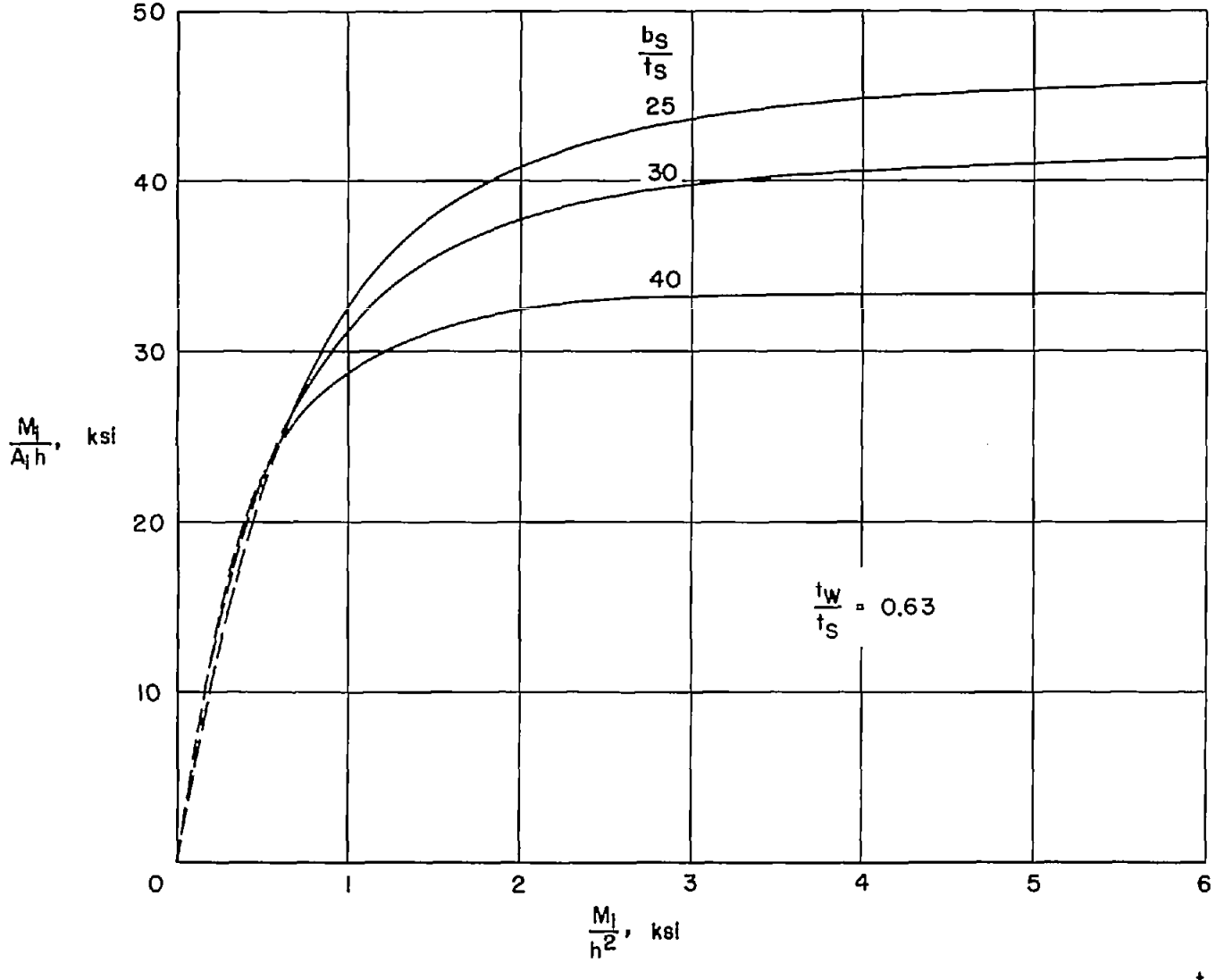

Figure 12. — Efficiency chart for 75S-T6 aluminum-alloy multiweb beams with formed-channel webs, $\frac{t_w}{t_s} = 0.63$.

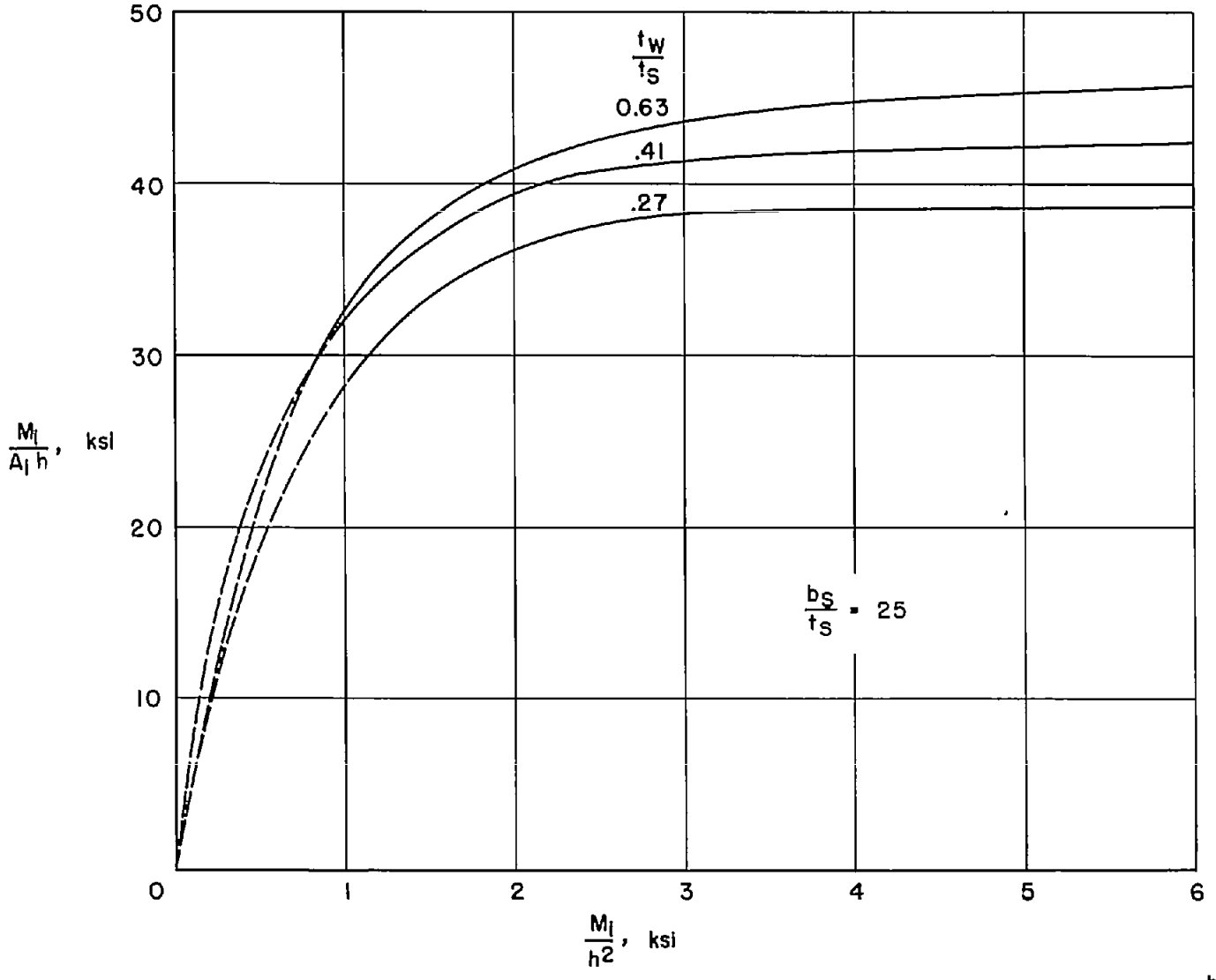

Figure 13.– Efficiency chart for 75S-T6 aluminum-alloy multiweb beams with formed-channel webs. $\frac{b_s}{t_s} = 25$.